Abdominal motion tracking with free-breathing XD-GRASP acquisitions using spatio-temporal geodesic trajectories

Rihab Mansour, M.Sc.[1], Liset Vazquez Romaguera, M.Sc.[2], Catherine Huet, M.Sc.[3] , Ahmed Bentridi, M.D.[3] ,Kim-Nhien Vu, M.D.[3],Jean-Sébastien Billiard, M.D., M.Sc.[3], Guilllaume Gilbert, Ph.D.[4], An Tang, M.D., M.Sc.[1, 3], Samuel Kadoury, Ph.D.[1, 2]

1 - Centre hospitalier de l'Université de Montréal (CHUM) Research center, Montréal, QC, Canada

2 - Department of Computer and Software Engineering, PO Box 6079, Polytechnique Montreal, Montréal, QC, Canada

3 - Department of Radiology, Centre hospitalier de l'Université de Montréal (CHUM), Montréal, QC, Canada

4 - MR Clinical Science, Philips Healthcare Canada.

Author biographies:

Rihab Mansour M.Sc. is a biomedical systems engineer and graduated from her Masters' degree in biomedical engineering in 2019. Her expertise is in MRI sequences and quality evaluations.

Liset Vazquez Romaguera M.Sc. is a Ph.D. candidate in Biomedical Engineering at Polytechnique Montreal. She completed her Masters' in Electrical Engineering at the Federal University of Amazonas in 2017.

Catherine Huet M.Sc. completed her Masters' in Preventive Nutrition at Université de Montréal in 2003 and in Human Nutrition at McGill University in 2011. She is a research agent at the CHUM Hospital in Montreal.

Ahmed Bentridi M.D. is an abdominal radiologist (U. Paris Descartes) and is currently a posy-doctoral fellow at the CHUM hospital in Montreal in interventional radiology.

Kim-Nhien Vu M.D. is an abdominal radiologist at the CHUM hospital in Montreal and associate professor of radiology at the University of Montreal.

Jean-Sébastien Billiard M.D., M. Sc. is a radiologist at the CHUM hospital in Montreal and associate professor of radiology at the University of Montreal.

Guillaume Gilbert Ph.D. is a MR clinical scientist at Philips Healthcare and an associate professor of radiology at University of Montreal. He completed his Ph.D. in physics in 2009 and specialises in MRI sequence development.

An Tang M.D., M. Sc. is a full professor of radiology at the University of Montreal and clinical researcher with an interest in imaging based diagnosis of focal and diffuse liver disease.

Samuel Kadoury Ph.D. is a full professor in biomedical engineering at Polytechnique Montreal and is the Canada Research chair in medical imaging and assisted interventions.

Corresponding author: Samuel Kadoury Ph.D.: samuel.kadoury@polymtl.ca

ABSTRACT

Free-breathing external beam radiotherapy remains challenging due to the complex elastic or irregular motion of abdominal organs, as imaging moving organs leads to the creation of motion blurring artefacts. In this paper, we propose a radial-based MRI reconstruction method from 3D free-breathing abdominal data using spatio-temporal geodesic trajectories, to quantify motion during radiotherapy. The prospective study was approved by the institutional review board and consent was obtained from all participants. A total of 25 healthy volunteers, 12 women and 13 men (38 years ± 12 [standard deviation]), and 11 liver cancer patients underwent imaging using a 3.0T clinical MRI system. The radial acquisition based on golden-angle sparse sampling was performed using a 3D stack-of-stars gradient-echo sequence and reconstructed using a discretized piecewise spatio-temporal trajectory defined in a low-dimensional embedding, which tracks the inhale and exhale phases, allowing the separation between distinct motion phases. Liver displacement between phases as measured with the proposed radial approach based on the deformation vector fields, were compared to a navigator-based approach. Images reconstructed with the proposed technique with 20 motion states and registered with the multiscale B-spline approach received on average the highest Likert scores for the overall image quality and visual SNR score 3.2 ± 0.3 (mean ± standard deviation), with liver displacement errors varying between 0.1 to 2.0 mm (mean 0.8 ± 0.6 mm). When compared to navigator-based approaches, the proposed method yields similar deformation vector field magnitudes and angle distributions, and with improved reconstruction accuracy based on mean squared errors.

I. INTRODUCTION

During abdominal radiation treatments, organ displacement induced by the patient's respiratory motion may affect dose delivery to tumor targets and cause collateral damages to surrounding healthy organs at risk [1]. Therefore, continuous organ tracking during irradiation of target tumors is required. Radiation oncologists generally rely on three dimensional (3D) images of the organs obtained before treatment and a few intra-procedural acquisitions. While there are several methods to non-rigidly align these multiple images, they only provide a static intraoperative representation due to the time required to perform the registration step [2]. Therefore, clinicians are unable to monitor in real time the patient's anatomical structures with these techniques. Recently, the combination of a linear accelerator (linac) with a magnetic resonance imaging (MRI) scanner, also known as MR-Linac, has enabled continuous organ visualization while the patient is being treated [3]. MRI-guided radiotherapy (MRgRT) [4] enables real-time MRI tracking during treatment and allows online dose calculation and replanning [5]. Moreover, it has the potential to improve treatment accuracy by monitoring the continuous changes of the tumor position [6]. However, due to spatio-temporal constraints, continuous 3D acquisitions do not provide an adequate temporal resolution to follow the respiratory motion. Instead, cine two dimensional (2D) slices are generally acquired during the course of treatment, disregarding the out-of-plane motion.

Multiple studies have assessed the feasibility of using orthogonal 2D acquisitions to estimate the 3D target motion through deformable registration . While this approach might be effective for local modeling [7], it is rather limited to estimate the entire anatomy. In contrast, motion models computed from dense motion data can be associated with the 2D cine imaging allowing for real-time 3D image generation [8][9] . To construct these models, the ground truth motion data is measured from 4D datasets via a deformable registration. Therefore, considerable efforts have been made to develop reconstruction methods providing 4D-MRI datasets. Indeed, since imaging volumes over time is not a feasible option, several alternative strategies have been proposed. Based on recent methods proposed in the literature, these can be classified in two groups: (1) retrospectively sorting of cine-slices and (2) full 3D acquisitions [10].

In the first category, 2D slices over several respiratory cycles are acquired simultaneously with either external or internal navigator signals [12]. These navigators are crucial for the subsequent slice reordering according to the respiratory phase, i.e. they allow to construct dynamic volumes with a temporal

consistency. Optical tracking devices and respiratory belts are examples of external navigators. However, these are known to suffer from low correlation with the internal organ motion, thereby causing artifacts in the obtained volumes. In contrast, internal navigators provide better information about the respiratory state at the cost of decreasing the temporal resolution. Other techniques, known as self-sorting or self-gating, have also been proposed to address the case where no navigator is available. Generally, they rely on deriving a motion signal using exclusively features contained in the images [13][14][15] or applying low-dimensionality reduction techniques [16][17]. The second category involves 3D readouts. In these methods, the readout type is directly related to the image quality, particularly in the presence of organ motion [10]. Over the past few years, the acquisition of radial k-space and compressed sensing with sparse temporal transforms has gained attention to enable high accelerations in dynamic MRI studies [18][19][20][21]. Moreover, since a reliable respiratory signal can be obtained directly from the raw k-space data, the self-navigation property is one of its advantages.

For certain studies, the compensation of the respiratory motion is required to increase image resolution. For instance, the iterative Golden-angle RAdial Sparse Parallel (GRASP) technique [22], and later the eXtra-Dimensional GRASP (XD-GRASP) [20], were proposed for motion-robust DCE-MRI. However these were designed to limit the impact of free-breathing motion, rather than exploit radial acquisitions to preserve motion during the post-acquisition processing in order to yield a respiratory-correlated dataset for radiotherapy applications. The XD-GRASP reconstruction method was extended with self-navigation based on reordering of slices in ascending or descending [11]. However, these were based on the matching of similar neighboring slices, without incorporating data-driven knowledge to the ordering process for modeling respiratory motion.

In this work, we introduce a novel image reconstruction method to obtain high-resolution dynamic 3D MRI data based on the XD-GRASP motion correction technique developed by Feng et al. [20]. Our approach models the respiratory cycle using piecewise geodesic trajectories in low-dimensional space to improve the ordering process of the motion phases, and generating 4D sequences across a respiratory cycle. While previous approaches performed image denoising with iterative backpropagation to improve 4D-MRI quality [23], these were focused on cardiac images and were not assessed by a panel of radiologists. In this study, we perform averaging through deformable registration, using the Likert score to qualitatively assess the quality of the produced images.

II. METHODS AND MATERIALS

A. Imaging datasets

In this study, abdominal image acquisitions were performed during free breathing on 25 healthy volunteers, 12 women and 13 men (38 years ± 12 [standard deviation]), between September and December 2019. The study was approved by our institutional review board and each participant provided their written informed consent. The MR scans were acquired using a 3.0T clinical MRI system (Ingenia, Philips Healthcare).

Each volunteer underwent two consecutive acquisitions, each one with different k-space readout: 3D radial and 2D cartesian. The radial acquisition was performed using a 3D stack-of-stars gradient-echo with balanced steady-state free precession (bSSFP) sequence with T2/T1 weighting rather than traditional T1 weighting. This contrast provides good visualization of blood vessels without contrast agent injection. This sequence offers near isotropic spatial resolution and a temporal resolution of approximately 200 ms. Data was acquired continuously during 8 minutes.

In the Cartesian acquisition, used as basis of comparison, sagittal cine-slices covering the right liver lobe interleaved with a navigator frame were acquired using a 2D balanced steady-state free precession (bSSFP) sequence with T2/T1 weighting without using any contrast agent. The navigator frame was positioned at the middle of the right hemi-diaphragm. Data was acquired in two consecutive blocks of 5 minutes each.

In addition to the two acquisitions acquired in volunteers, we have also analyzed a previously acquired dynamic contrast-enhanced (DCE)-MRI dataset during free breathing in 11 liver cancer patients, 5 women and 6 men (70 years ± 11 [standard deviation]), diagnosed with HCC. Patients have previously provided a written consent for the prospective study and retrospective analysis was approved by our institutional review board. The recruitment process followed on this dataset can be found in [31]. This data was acquired for 3 minutes with the same aforementioned clinical MRI system using the same 3D radial stack-of-stars gradient-echo sequence between September and December 2018. Imaging parameters for all sequences are listed in **Table I**.

B. Free-breathing 4D-MRI reconstruction with geodesic trajectories

XD-GRASP is a dynamic image reconstruction approach based on reconstructing the extra dimension of respiratory motion obtained from k-space data acquired during free breathing [20]. It is usually achieved by ordering the respiratory motion

from end-inspiration to end-expiration and then dividing it into several respiratory motion states, with the same number of spokes in each motion state. While XD-GRASP attempts to reduce the impact of breathing motion, the proposed approach aims to preserve it.

The goal of the proposed method is to locate precisely each data sample from the center of k-space data, within the respiratory motion trajectory from inspiration to expiration, thus avoiding a binary inhale/exhale separation. To accomplish this, each k-space sample point is embedded into a pre-trained latent embedding which captures the global motion. The sorted mapped values are then used to construct a respiratory navigator signal, alternating between inhale and exhale phases **(Fig.1)**.

The mapping process of the acquired k-space data into a latent space is based on a kernel embedding method [32], modeling the spatiotemporal evolution of breathing patterns during 4D-MRI acquisitions. The curve embedding is generated from a training set of K_d samples measured t_N times, where for each sample k_i, it selects neighbors $k_{i,j}$ showing similar breathing patterns in the training set from pre-treatment models within latent space, yielding neighborhoods $\mathbb{N}(k_{i,t})$ with data-points across the breathing motion continuum. Hence, a Riemannian space from samples $k_{i,t}$ is created, with each patient model i acquired at time t ($t=0$ as the baseline, denoted $k_{i,0}$). Assuming the domain manifold is well represented and the piecewise-geodesic curve spanning the time spectrum, a regression of the labelled samples can be obtained in $\Re^D$, generating regular paths in the spatio-temporal domain $\Re^d$. A discretized regression technique is used [33] for implementation purposes of the piecewise trajectory. The geodesic path is obtained from the neighborhoods of samples obtained along γ, by optimizing a loss function which minimizes the geodesic distance between the K_d samples and the regressed curve, as well as the L2 metric of the first and second derivatives of γ:

$$E(\gamma) = \frac{1}{K_d}\sum_{i=1}^{K_d}\sum_{j=0}^{t_N} w_i \parallel \gamma(t_{i,j}) - \left(k_{i,j} - \left(k_{i,0} - k_q\right)\right) \parallel^2 + \frac{1}{2}\sum_{i=1}^{K_d} \alpha_i \parallel v_i \parallel^2 + \frac{1}{2}\sum_{i=1}^{K_d} \beta_i \parallel a_i \parallel^2 \quad (1)$$

where w_i weights the differences between the samples inferred from the geodesic-inferred k-space γ and the ground-truth data. The last two terms capture the velocity v_i (weighted with α) and acceleration a_i (weighted with β) of the regressed path, which ensures a continuous curve with smooth transitions during changes of direction. This allows for a query sample k_q to navigate through the respiratory motion path, capturing the average deformable transformations linked to motion, which are obtained from N training cases. Eq.(1) is minimized using a non-linear conjugant gradient descent technique. Once the piecewise geodesic trajectory is

generated, new samples can be mapped to define their order in the reparation cycle.

During the acquisition phase, the noise levels of the coil elements used for signal reception may vary. Therefore, to eliminate the effect of the non-optimal placement of coil elements relative to subjects, a noise whitening step, which normalizes and decorrelates the noise, was applied to the k-space data.

The pulse sequence used in this study represents a stack-of-stars trajectory with radial sampling over k_x-k_y, where the sampling angle is the golden angle ~111.25°, and Cartesian encoding over k_z [24]. Since this oversampling can result in overweighting low frequencies, a density compensation is used, which accomplishes the same purpose as a ramp filter [25]:

$$d(\emptyset, r) = |r| * \frac{1}{N}, \quad (2)$$

where N *is* the number of radial samplings and r is the k-space data.

Finally, during the pre-processing steps, the coil sensitivity is an important parameter to estimate. For this purpose, and to reduce noise in the images background, the Walsh approach [26] was adapted. Such an approach applies an adaptive matched filter for the multi-coil data. The noise and signal covariance matrices were determined for each image pixel, where an optimal estimation of the coil sensitivity was provided by the eigenvector of the matrices. The individual coil images used to estimate the sensitivity were extracted by computing the non-uniform fast Fourier transform (NUFFT) on the radial k-space data.

As a result, one breathing cycle was obtained from the 8-minutes acquisition described in the previous section. It was then divided into 20 respiratory motion states, i.e. 10 temporal points between extreme phases (expiration-inspiration-expiration). Once inspiration and expiration phases were differentiated, the liver data was reconstructed by solving the optimization equation using compressed sensing as implemented by Feng et al. [20]. The same process was applied for the 3-minutes acquisition performed on patients. However, in this case 10 motion states were reconstructed instead of 20. All the reconstructions were performed in MATLAB R2018a (The MathWorks, Inc., Natick, MA, USA).

C. Non-rigid registration step

In order to improve the image quality of the reconstructed radial images, we adopted the following methodology **(Fig. 2)**. All motion states, i.e. the temporal volumes, were non-rigidly registered to a reference volume (3D static image), which was initially chosen as the first acquired image in the temporal sequence. Then, the resulting deformations were averaged. This process was repeated while varying the

reference to be each one of the 20 volumes obtained from the 8-minutes acquisition. Two registration approaches were tested and compared:

1. *Multi-scale B-splines (MSBS)*
   In this approach, a transformation model based on cubic B-splines with a pyramidal multi-resolution strategy at three different levels was applied as implemented in the Elastix framework [27]. The Normalized Mutual Information was used as a similarity metric to quantify the alignment between target and source volumes. This deformable registration was initialized with a rigid body transformation, also performed in Elastix.

2. *Subpixel deformation maps (SPDM)*
   This method is based on non-rigid motion compensation using subpixel deformation maps. It estimates a non-rigid displacement by computing an optical flow formula adapted to perfusion series dynamics. This application was able to register the MR image series with different respiratory patterns [28][29]. The optimal deformable registration field w is computed by minimizing the following cost function:

$$E(w) = \lambda E_{grad}(w) + E_{int}(w) + \mu E_{smooth}(w) + +E_{desc}(w_1) + \eta E_{match}(w, w_1) \quad (3)$$

where E_{grad} represents the gradient constraint, E_{int} represents the pixel intensity energy term, E_{smooth} is the regularization term, E_{desc} is a continuous formulation for the discrete descriptor matching and E_{match} is a histogram-oriented gradient (HOG) based on landmark correspondences. Additionally, three parameters control this equation: λ got the gradient consistency term, μ for the smoothness of flow fields, and η for the HOG descriptor matching term. For the deformable registration method, parameters were set as λ=0.05, μ=0.4 and η=0.1 based on empirical evaluations.

D. Evaluation methodology

To compare the proposed 4D-MRI reconstruction approach before and after applying the registration methods, three fellowship-trained abdominal radiologists, blinded to any technical details on the type of images (with or without registration and type of registration), assessed the healthy volunteers' images after randomization. A visual scoring, using a five-point Likert scale, was assigned to each image depending on its quality. The grading scale used a quality index: 1 (extremely poor) and 2 (poor) were considered as clinically unacceptable, while 3

(fair), 4 (good), and 5 (excellent) were clinically acceptable [30]. The readers then used the same 5-point rating scale to grade the visual signal-to-noise ratio (SNR).

A quantitative analysis was also conducted by computing the deformation between volumes at extreme phases. This step aimed at estimating the maximum liver displacement. The displacement vector fields (DVF) yielded by the deformable registration were multiplied by a liver segmentation mask. Subsequently, the three-dimensional Euclidean distance was calculated over the DVF as follows:

$$d = \sqrt{(\Delta_X)^2 + (\Delta_Y)^2 + (\Delta_Z)^2} \quad (3)$$

where *x*, *y* and *z* represents the voxel-wise displacements in the three-dimensional space. The distribution of magnitudes and angles over the set of displacement vectors was calculated.

Finally, target registration errors based on Euclidean distances in landmarks identified by the experienced radiologists were calculated between the initial and final motion phases for the different registration approaches, and are shown for each volunteer subject.

E. Comparison with 4D-MRI reconstruction methods

The proposed 4D reconstruction method was compared to a well-established technique, based on 2D navigators [15]. During the imaging process explained in section A, we followed an interleaved scheme to acquire two types of slices. The first ones covered consecutive liver locations up to imaging the whole area of interest. The second one was a navigator frame, taken at a fixed anatomical position, which was selected at the middle of the right hemi-diaphragm. Since the navigator frames are common for all the data slices (regardless of their anatomical position), they act as a reference, which is the key for the slice reordering. For instance, two data frames acquired at different anatomical positions can be stacked together if their navigator frames are similar, which means that they correspond to the same respiratory phase.

The first step for the reconstruction was the segmentation of a master navigator, which can be selected at any respiratory phase. Manual segmentation was performed by an experienced radiologist, using the MITK software (v2021.02) which uses an interactive tool allowing to draw curves snapping to the liver edges. In our case, the master navigator was selected as the middle phase (i.e. mid-exhale or mid-inhale). The liver segmentation was conducted manually to ensure the best results. The second step is to non-rigidly register all the navigator slices to the master navigator. This deformable registration was initialized with a rigid transformation to cope with large displacements and conducted using the multi-

scale B-splines model and normalized mutual information similarity metric as implemented in the Elastix framework [14]. Then, the 2D dense displacement fields were multiplied by the segmentation mask. Finally, the resulting values were used to compute a cost function to guide the slice stacking, as described in [15]. The temporal resolution of the dynamic volumes was 450 ms. This reconstruction process yielded a time-resolved dataset, covering several respiratory cycles. In order to enable a fair comparison with the single respiratory cycle yielded by the proposed method, we computed an average cycle from the volumes of this dataset. Furthermore, the volumes from the healthy volunteers were cropped to the smaller field of view, which correspond to the one acquired by the multi-slice Cartesian acquisition. We also compared the proposed technique to two other reconstruction techniques, namely, the original XD-GRASP method based on compressed sensing for 4D k-space regularization method [20], and a self-navigation method based on reordering of slices, inspired by [11].

F. Statistical analysis

Statistical analyses were performed by a biostatistician (23 years of experience) (Software Stata/IC version 14.2). Wilcoxon tests were performed for paired sample analysis. Here, p values < 0.05 were considered significant for this study.

III. RESULTS

A. Image quality

Fig. 3 shows a comparison of the image quality and the visual SNR score achieved with the original XD-GRASP and our proposed method using the two different registration approaches. These values were obtained for each case by visual grading. In most cases, the integration of a deformable registration step, regardless of its type, yielded better results than the original approach, which does not include such step. Furthermore, it can be observed that the volumes reconstructed with the proposed approach and registered with the MSBS approach, obtained the best quality scores and higher visual SNR score values compared to the other two alternatives. Therefore, this type of registration is more suitable than the one based on subpixel deformation maps. The mean overall image quality and visual SNR score was of 3.2 ± 0.3 and 3.4 ± 0.3 [mean ± standard deviation], 2.30± 0.4 and 2.4 ± 0.3, and 2.0 ± 0.4 and 1.9 ± 0.3 for the MSBS, SPDM and original approaches,

respectively. The MSBS approach yielded a statistically significant improvement in Likert and SNR metrics to other approaches ($p < 0.05$).

A visual example of these results is illustrated for 4 cases in **Fig. 4**. Compared to the original reconstruction without registration, the introduction of the MSBS approach demonstrates reduced imaging artefacts and improved contrast which enhances overall image quality.

B. Liver displacement

Fig. 5 (a) illustrates the liver motion between motion states and compares the reconstruction approaches before and after registration. The white lines indicate the diaphragm boundaries. The deformation vectors and their magnitudes and angles confirm that there is a clear motion between different states and how it differs between registration approaches (see **Fig 5 (b)**).

Fig. 6 (a) compares the mean vector-wise Euclidean distance estimated between inhalation and exhalation for each volunteer. The distance without registration varies between 9 mm and 32 mm (mean 16.2 $\pm$ 7.3 mm). When applying the MSBS and SPDM registration approaches, the values range between 8 mm and 31 mm (mean 16.1 $\pm$ 7.1 mm) and between 5 mm and 24 mm (mean 10.1 $\pm$ 4.8 mm), respectively. These values, however, depend on the respiratory motion of each volunteer.

To estimate the motion errors between each method and the original images without any registration, the difference between them was calculated as shown in **Fig. 6 (b).** The errors for the first method varies between 0.1 and 2.0 mm (mean 0.8 $\pm$ 0.6 mm) while for the second method, it varies between 1.8 to 20.0 mm (mean 8.2 $\pm$ 5.5 mm). We can clearly see the similarity between the original images before and after registration with the first approach based on multi-scale B-splines. The registration should not affect the motion amplitude but this difference is due to registering the 20 motion states and then averaging it using a non-rigid method. The errors generated with the MSBS method were statistically significant lower to the SPDM approach.

Finally, target registration errors were calculated between the initial and final motion phases, and are shown for each volunteer subject in **Fig. 7.** Overall, the results yield a TRE of 1.7 $\pm$ 1.5mm with the MSBS method, compared to 4.4 $\pm$ 3.4mm with the SPDM method, leading to a statistically significant improvement ($p < 0.05$) based on Wilcoxon tests.

An analysis of the effect of uncertainties due to errors from the deformable registration process was performed, by analyzing cases which were in the 90th percentile of residual errors in the deformable registration step. This showed that

target registration errors were significantly higher based on a two-tailed Student t-test ($p<0.05$) for that group of cases.

435

C. Comparison to 4D-MRI reconstruction techniques

The deformation fields were calculated based on the Elastix visualization toolkit to compare the navigator-based and proposed methods as shown in **Fig. 8**, as well as the corresponding DVF magnitude and angle distribution of all volunteers was represented in **Fig. 9**. The two methods show almost similar DVF magnitudes and angles distribution. The difference between the two methods is due to the fact that the data was acquired at different times and thus different respiratory movement.

Table II presents a quantitative comparison of the proposed 4D-MRI reconstruction method to other benchmark methods presented in section II.E. Results show an improvement in the mean square error MSE measures and peak-signal-to-noise ratio (PSNR), which is between intensity values of the reconstructed 4D-MRI and original dataset. Both metrics saw a statistically significant improvement ($p < 0.05$) with the MSBS approach. We also calculate the mean structural similarity (MSSIM) index, which does not consider the intensity difference, but allows us to evaluate the contrast level and the anatomical structure of the 4D-MRI compared to the reference.

D. Application to patient data

Finally, in order to test the performance of our technique in patients treated for liver cancer, the proposed method was evaluated on 11 separate patients with HCC, by including a total of 10 motion states and followed by a registration based on the multi-scale B-splines approach. **Fig. 10** shows images of 4 different patients at 3 different motion states. The liver motion is clear where we can see the different position of the liver and tumors. Because of the inherent variability between patients which may cause tumor enhancement to appear differently in others due to contrast injection, this may impact the Likert scores. Therefore, to avoid this bias, we chose to perform image quality evaluation only on healthy cases, where no HCC enhancement was present and only the image quality of the liver anatomy can be objectively evaluated.

E. Computational time

The proposed method required 10 hours to reconstruct the 20 volumes of each subject when implemented on a CPU Intel® Core™ i7-8700 with 3.2 GHz and 32 Gb RAM. Half of this total time corresponded to the actual k-space reconstruction, whereas the other half was related to the registration step. The manifold model creation is performed once, offline. It should be noted that reconstructing 20 phases involves 400 deformable registrations, which is time-consuming. Thus, this process was parallelized.

IV. DISCUSSION

From the experiments performed in this study, several aspects of the method based on the piecewise geodesic motion trajectory were shown to be beneficial compared to similar free-breathing reconstruction methods. These experiments were performed on both volunteer and patient data, evaluated both qualitatively (from a panel of experienced radiologists) and quantitatively using landmark tracking errors, as well as image fidelity metrics.

Firstly, the respiratory signal used for the ordering process is extracted from the geodesic trajectory constructed from k-space data. This physiological signal is more reliable and robust than those acquired with external devices, such as respiratory belts or optical trackers. Moreover, it is less prone to artifacts during the imaging process. Secondly, since the proposed method uses a 3D acquisition, an exhaustive sampling is no longer required to capture all the potential states of the imaged organs used for the navigator-based approach. For instance, to ensure an accurate stacking of slices from the left liver lobe, it is important to capture most of the possible combinations of heart and respiratory motions. Otherwise, the volumes would be affected by artifacts due to misordered slices or spatiotemporal inconsistencies. In fact, this exhaustive sampling is one of the key assumptions that supports the multi-slice acquisition approach. Consequently, it requires longer acquisition sessions, which might be uncomfortable for subjects due to the noise and warm temperatures inside the scanner. On the other hand, during the treatment planning for external beam radiotherapy, 4D datasets containing an average cycle are generally acquired. These scans are very likely to present artifacts such as blurring [34], duplication, overlapping, and incompletion [35]. Also, it represents an extra burden of ionizing radiation to the patient. In contrast, our proposed method enables an accurate reconstruction of an average respiratory cycle from an MRI sequence lasting only a few minutes and providing excellent soft tissue contrast without ionizing radiation. This work was made towards providing a single, personalized 4D sequence of the entire abdominal region before radiation therapy

begins. In this type of workflow, the sequence would be generated and processed just before administering therapy and used to anticipate motion. Other types of workflows require on the other hand real-time volumetric imaging. In related efforts, deep learning has been explored for real-time imaging, integrating predictive components by learning the relationship in deformation fields between surrogate navigators such as in-plane 2D images and 3D volumes [36][37]. This allows to generate volumes within a 1 s horizon, respecting system latencies.

Several parameters dictate the behavior of the method's performance. For example, the number of temporally averaged images (n=20) is set during the acquisition phase, and is found as a compromise between temporal resolution and time to perform acquisitions. The cut-off frequency of the used filters was determined empirically based on a proper balance between image smoothness and vessel visibility. With regards to the weights and smoothness terms in Eq. (3), the impact of the gradient consistency term weight λ will be seen mostly on the edges and liver boundaries, while the smoothness term μ for the flow fields will mostly impact the deformation fields. Finally, the weight for the HOG descriptor matching term η will impact the similarity between similar samples.

Spontaneous motion can be the cause of severe artifacts due to the sudden changes in appearance of the anatomy which may deviate from the learned trajectories. This aspect is handled from two factors. The first is the smoothness term controlled in Eq. (3), where the deformable registration process will ensure that the DVF will be regular when averaging the images together to a common space, thereby reducing the adverse effects of outliers. The other is the piecewise geodesic trajectory in latent space, which ensures mapped data is regular within the respiratory motion model.

Unlike the compared 2D navigator-based method, our approach is fully automated. It does not require the manual selection of a master navigator slice. Another potential weakness of previous approaches is the fact they are based primarily on displacement vector fields computed through non-rigid registration between pairs of slices. This process depends on the cost function which may be sensitive to out of plane motion. Nevertheless, the registration is a challenging task that is not exempt from errors, mainly due to uncertainties during the image acquisition. Consequently, it may appear as potential errors during the stacking that are often reflected on morphological inaccuracies, such as irregular organ boundaries or truncated vessels. In contrast, since the proposed approach is reconstructs images directly from the k-space, we obtain smoother organ boundaries and sharp appearance of the vessels.

Compared to the original XD-GRASP, the proposed approach allows to significantly improve the image quality as assessed by radiologists, and improves the deformation fields with the introduction of a deformable registration method within the reconstruction pipeline. Currently, one of the study's limitations is the time for 4D reconstruction, which can take several hours, depending on the computational resources. In the scenario where the volumes are acquired just before therapy, this may be more challenging.

V. CONCLUSION

In conclusion, we presented a method for dynamic volume reconstruction from free-breathing MRI acquisitions, which is based on the original golden angle radial acquisition technique [20], but tailored for quantifying abdominal motion during free-breathing acquisitions. This helps to improve target tracking for radiotherapy applications. We introduced a new technique for mapping the k-space data to a piecewise geodesic curve trajectory of the respiratory motion, thus allowing the reconstruction of multiple motion phases in one cycle. In addition, we integrated a deformable registration step to further enhance the visual quality of the volumes. The proposed method was compared to well-established free-breathing reconstruction techniques based on navigator frames. Results showed that the method can achieve similar performance while introducing important advantages. Moreover, these advantages prevail when compared to other reconstruction techniques based on the multi-slice acquisition approach, regardless of the type of navigator employed.

Future work will consist of evaluating the framework in a radiotherapy context, using free-breathing acquisitions to evaluate prospectively the ability to track tumors during respiration compared to intermittent volumetric acquisitions. We will also explore possibilities to reduce the computational complexity by parallelizing all components of the reconstruction process, including the k-space reconstruction, thereby requiring minimal time to generate the personalized 4D motion model.

Declarations: Funding for this study was provided by the National Science and Engineering Research Council of Canada (CRDPJ-517413-17), MEDTEQ and the Cancer Research Society of Canada. Dr. An Tang was supported by the Fonds de recherche du Québec - Santé and the Fondation de l'Association des Radiologistes du Québec (Career Award #34939).

RM wrote the manuscript, developed the proposed models and conducted the experiments. LVR provided additional experiments. CH performed patient recruitement. AB, KV and JSB provided radiological evaluation and helped write the manuscript. GB provided MRI expertise. AT provided the clinical context and helped write the manuscript. SK assisted with oversight of the project and helped write the manuscript.

Competing interests statement: Author G. Gilbert is an employee of Philips. All other author shave no conflicts of interest associated with this publication.

Ethical statement: All procedures performed in studies involving human participants were in accordance with the ethical standards of the institutional and/or national research committee and with the 1964 Helsinki declaration and its later amendments or comparable ethical standards. Ethics approval was granted by the Institutional Review Board (IRB) for human studies of the Centre Hospitalier Université de Montréal (CHUM). Informed patient consent was obtained through an IRB approved protocol at CHUM (# 15.388) to use imaging data.

Informed consent: All participants provided their formal consent to participate in this study.

References:

[1] Balter, J. M., Ten Haken, R. K., Lawrence, T. S., Lam, K. L., & Robertson, J. M. (1996). Uncertainties in CT-based radiation therapy treatment planning associated with patient breathing. *International Journal of Radiation Oncology* Biology* Physics*, *36*(1), 167-174.

[2] Sotiras, A., Davatzikos, C., & Paragios, N. (2013). Deformable medical image registration: A survey. *IEEE Transactions on Medical Imaging*, *32*(7), 1153-1190.

[3] Mutic, S., & Dempsey, J. F. (2014, July). The ViewRay system: magnetic resonance–guided and controlled radiotherapy. In *Seminars in Radiation Oncology* (Vol. 24, No. 3, pp. 196-199). WB Saunders.

[4] Paganelli, C., Summers, P., Gianoli, C., Bellomi, M., Baroni, G., & Riboldi, M. (2017). A tool for validating MRI-guided strategies: a digital breathing CT/MRI phantom of the abdominal site. *Med Biol Eng Comput,* 55, 2001-2014.

[5] Mzenda, B., Hosseini-Ashrafi, M., Palmer, A., Liu, H., & Brown, D.J. (2010). A simulation technique for computation of the dosimetric effects of setup, organ motion and delineation uncertainties in radiotherapy. *Med Biol Eng Comput*, 48, 661-669.

[6] Wojcieszynski, A. P., Rosenberg, S. A., Brower, J. V., Hullett, C. R., Geurts, M. W., Labby, Z. E., & Bassetti, M. F. (2016). Gadoxetate for direct tumor therapy and tracking with real-time MRI-guided stereotactic body radiation therapy of the liver. *Radiotherapy and Oncology*, *118*(2), 416-418.

[7] Miranda, A., Staelens, S., Stroobants, S., & Verhaeghe, J. (2019). Estimation of and correction for finite motion sampling errors in small animal PET rigid motion correction. *Med Biol Eng Comput*, 57, 505-518.

[8] Zhang, Q., Pevsner, A., Hertanto, A., Hu, Y. C., Rosenzweig, K. E., Ling, C. C., & Mageras, G. S. (2007). A patient-specific respiratory model of anatomical motion for radiation treatment planning. *Medical Physics*, *34*(12), 4772-4781.

[9] Garau, N., Via, R., Meschini, G., Lee, D., Keall, P., Riboldi, M., & Paganelli, C. (2019). A ROI-based global motion model established on 4DCT and 2D cine-MRI data for MRI-guidance in radiation therapy. *Physics in Medicine & Biology*, *64*(4), 045002.

[10] Stemkens, B., Paulson, E. S., & Tijssen, R. H. (2018). Nuts and bolts of 4D-MRI for radiotherapy. *Physics in Medicine & Biology*, *63*(21), 21TR01.

[11] Stemkens, B., Prins, F. M., Bruijnen, T., Kerkmeijer, L. G., Lagendijk, J. J., van den Berg, C. A., & Tijssen, R. H. (2019). A dual-purpose MRI acquisition to

combine 4D-MRI and dynamic contrast-enhanced imaging for abdominal radiotherapy planning. *Physics in Medicine & Biology*, *64*(6), 06NT02.

[12] Tryggestad, E., Flammang, A., Han-Oh, S., Hales, R., Herman, J., McNutt, T. & Wong, J. (2013). Respiration-based sorting of dynamic MRI to derive representative 4D-MRI for radiotherapy planning. *Medical Physics*, 40(5), 051909.

[13] Tong, Y., Udupa, J. K., Ciesielski, K. C., Wu, C., McDonough, J. M., Mong, D. A., & Campbell Jr, R. M. (2017). Retrospective 4D MR image construction from free-breathing slice acquisitions: A novel graph-based approach. *Medical Image Analysis*, *35*, 345-359.

[14] van de Lindt, T., Sonke, J. J., Nowee, M., Jansen, E., van Pelt, V., van der Heide, U., & Fast, M. (2018). A self-sorting coronal 4D-MRI method for daily image guidance of liver lesions on an MR-LINAC. *International Journal of Radiation Oncology* Biology* Physics*, *102*(4), 875-884.

[15] Romaguera, L. V., Olofsson, N., Plantefève, R., Lugez, E., De Guise, J., & Kadoury, S. (2019). Automatic self-gated 4D-MRI construction from free-breathing 2D acquisitions applied on liver images. *International Journal of Computer Assisted Radiology and Surgery*, *14*(6), 933-944.

[16] Baumgartner, C. F., Gomez, A., Koch, L. M., Housden, J. R., Kolbitsch, C., McClelland, J. R., & King, A. P. (2015, June). Self-aligning manifolds for matching disparate medical image datasets. In *International Conference on Information Processing in Medical Imaging* (pp. 363-374). Springer, Cham.

[17] Clough, J. R., Balfour, D. R., Marsden, P. K., Prieto, C., Reader, A. J., & King, A. P. (2018, April). MRI slice stacking using manifold alignment and wave kernel signatures. In *2018 IEEE 15th International Symposium on Biomedical Imaging (ISBI 2018)* (pp. 319-323). IEEE.

[18] Han, F., Zhou, Z., Du, D., Gao, Y., Rashid, S., Cao, M., & Hu, P. (2018). Respiratory motion-resolved, self-gated 4D-MRI using Rotating Cartesian K-space (ROCK): Initial clinical experience on an MRI-guided radiotherapy system. *Radiotherapy and Oncology*, *127*(3), 467-473.

[19] Deng, Z., Pang, J., Yang, W., Yue, Y., Sharif, B., Tuli, R., & Fan, Z. (2016). Four-dimensional MRI using three-dimensional radial sampling with respiratory self-gating to characterize temporal phase-resolved respiratory motion in the abdomen. *Magnetic Resonance in Medicine*, *75*(4), 1574-1585.

[20] Feng, L., Axel, L., Chandarana, H., Block, K. T., Sodickson, D. K., & Otazo, R. (2016). XD-GRASP: golden-angle radial MRI with reconstruction of extra motion-state dimensions using compressed sensing. *Magnetic Resonance in Medicine*, *75*(2), 775-788.

[21] Küstner, T., Fuin, N., Hammernik, K., Bustin, A., Qi, H., Hajhosseiny, R., & Prieto, C. (2020). CINENet: deep learning-based 3D cardiac CINE MRI

reconstruction with multi-coil complex-valued 4D spatio-temporal convolutions. *Scientific Reports*, *10*(1), 1-13.

[22] Feng, L., Grimm, R., Block, K. T., Chandarana, H., Kim, S., Xu, J., & Otazo, R. (2014). Golden-angle radial sparse parallel MRI: combination of compressed sensing, parallel imaging, and golden-angle radial sampling for fast and flexible dynamic volumetric MRI. *Magnetic Resonance in Medicine*, *72*(3), 707-717.

[23] de Senneville, B. D., Cardiet, C. R., Trotier, A. J., Ribot, E. J., Lafitte, L., Facq, L., & Miraux, S. (2020). Optimizing 4D abdominal MRI: image denoising using an iterative back-projection approach. *Physics in Medicine & Biology*, *65*(1), 015003.

[24] Usman, M., Atkinson, D., Odille, F., Kolbitsch, C., Vaillant, G., Schaeffter, T., & Prieto, C. (2013). Motion corrected compressed sensing for free-breathing dynamic cardiac MRI. *Magnetic Resonance in Medicine*, *70*(2), 504-516.

[25] Fessler, J. A., & Sutton, B. P. (2003). Nonuniform fast Fourier transforms using min-max interpolation. *IEEE Transactions on Signal Processing*, *51*(2), 560-574.

[26] Lustig, M., Donoho, D., & Pauly, J. M. (2007). Sparse MRI: The application of compressed sensing for rapid MR imaging. *Magnetic Resonance in Medicine: An Official Journal of the International Society for Magnetic Resonance in Medicine*, *58*(6), 1182-1195.

[27] Klein, S., Staring, M., Murphy, K., Viergever, M. A., & Pluim, J. P. (2009). Elastix: a toolbox for intensity-based medical image registration. *IEEE Transactions on Medical Imaging*, *29*(1), 196-205.

[28] Benovoy, M., Jacobs, M., Cheriet, F., Dahdah, N., Arai, A. E., & Hsu, L. Y. (2017). Robust universal nonrigid motion correction framework for first-pass cardiac MR perfusion imaging. *Journal of Magnetic Resonance Imaging*, *46*(4), 1060-1072.

[29] Jacobs, M., Benovoy, M., Chang, L. C., Arai, A. E., & Hsu, L. Y. (2016). Evaluation of an automated method for arterial input function detection for first-pass myocardial perfusion cardiovascular magnetic resonance. *Journal of Cardiovascular Magnetic Resonance*, *18*(1), 1-11.

[30] Martinez, J. A., Moulin, K., Yoo, B., Shi, Y., Kim, H. J., Villablanca, P. J., & Ennis, D. B. (2020). Evaluation of a workflow to define low specific absorption rate MRI protocols for patients with active implantable medical devices. *Journal of Magnetic Resonance Imaging*, *52*(1), 91-102.

[31] Mansour, R., Antonacci, A. T., Bilodeau, L., Romaguera, L. V., Cerny, M., Huet, C., & Kadoury, S. (2020). Impact of temporal resolution and motion correction for dynamic contrast-enhanced MRI of the liver using an accelerated golden-angle radial sequence. *Physics in Medicine & Biology*, *65*(8), 085004.

[32] Schiratti, J. B., Allassonniere, S., Colliot, O., & Durrleman, S. (2015, December). Learning spatiotemporal trajectories from manifold-valued longitudinal data. In *Neural Information Processing Systems* (No. 28).

[33] Boumal, N., Absil, P.A. (2011). A discrete regression method on manifolds and its application to data on SO (n). IFAC Proceedings Volumes 44(1) 2284-2289.

[34] Tarroni, G., Tersi, L., Corsi, C., & Stagni, R. (2012). Prosthetic component segmentation with blur compensation: a fast method for 3D fluoroscopy. *Med Biol Eng Comput,* 50, 631-640.

[35] Yamamoto, T., Langner, U., Loo Jr, B. W., Shen, J., & Keall, P. J. (2008). Retrospective analysis of artifacts in four-dimensional CT images of 50 abdominal and thoracic radiotherapy patients. *International Journal of Radiation Oncology* Biology* Physics*, *72*(4), 1250-1258.

[36] Romaguera, L. V., Mezheritsky, T., Mansour, R., Carrier, J. F., & Kadoury, S. (2021). Probabilistic 4D predictive model from in-room surrogates using conditional generative networks for image-guided radiotherapy. *Medical Image Analysis*, 102250.

[37] Mafi, M., & Moghadam, S.M. (2020). Real-time prediction of tumor motion using a dynamic neural network. *Med Biol Eng Comput*, 58, 529-539.

TABLES AND FIGURES

TABLE I: Sequences parameters used to acquire imaging volumes of both healthy volunteers and liver cancer patients. Two sequences were used for each volunteer, one radial acquisition for the proposed method, and one Cartesian acquisition for basis of comparison.

	Sequence Parameter	
25 Healthy Volunteers	**Radial acquisition**	
	Sequence type	3D radial stack-of-stars gradient-echo acquisition with bSSFP
	Plane	Axial
	Contrast weighting	T2/T1
	Flip angle	20°
	Repetition time	2.3 ms
	Echo time	1.5 ms
	Spatial resolution	2 x 2 x 2.5 mm
	Cartesian acquisition	
	Sequence type	2D bSSFP contrast
	Plane	Sagittal
	Contrast weighting	T2/T1
	Flip angle	50°
	Repetition time	2.86 ms
	Echo time	1.43 ms
	Spatial resolution	1.7 x 1.7 x 3.5 mm
11 Patients	**DCE-MRI sequence**	
	Sequence type	3D stack-of-stars gradient-echo radial acquisition with fat saturation
	Plane	Axial
	Contrast weighting	T1
	Flip angle	12°
	Repetition time	3.40 ms
	Echo time	1.40 ms
	Spatial resolution	1.5 x 1.5 x 2.5 mm

765 **TABLE II:** Comparison of the proposed 4D-MRI reconstruction technique with the original XD-GRASP using compressed sensing [20], a 2D-based navigator approach [15] and the self-navigation method based on reordering of slices [11]. MSE: mean square error; PSNR: peak-signal-to-noise ratio; MSSIM: mean structural similarity. Bold values indicate statistically significant differences.

770

	MSE (mm)	**PSNR score**	**MSSIM**
XD-GRASP [23]	23.76 ± 0.20	19.44 ± 0.36	0.74 ± 0.35
2D navigator [28]	19.62 ± 0.20	23.71 ± 0.31	0.80 ± 0.30
Slice reordering [15]	15.57 ± 0.19	26.19 ± 0.27	0.83 ± 0.25
Proposed	**13.45 ± 0.18**	**30.89 ± 0.17**	0.87 ± 0.18

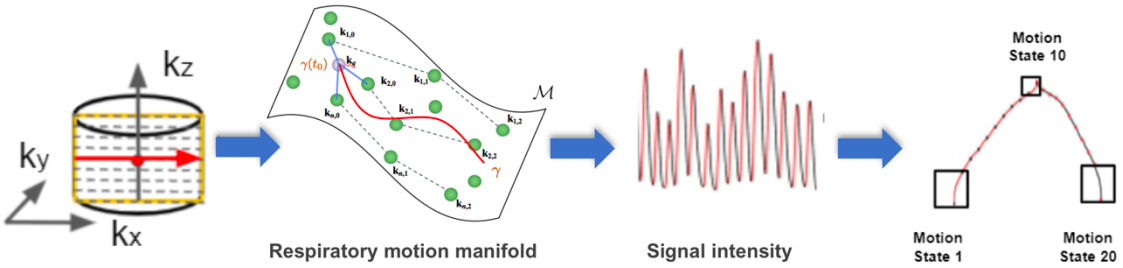

Figure 1. Proposed 4D-MRI reconstruction method based on the XD-GRASP method and a respiration motion model from a manifold embedding. Data is extracted from the center of k-space and is mapped onto a low-dimensional embedding, describing the relationship between neighboring samples in the breathing cycle. The trained model is used to extract the respiratory motion signal for slice re-ordering.

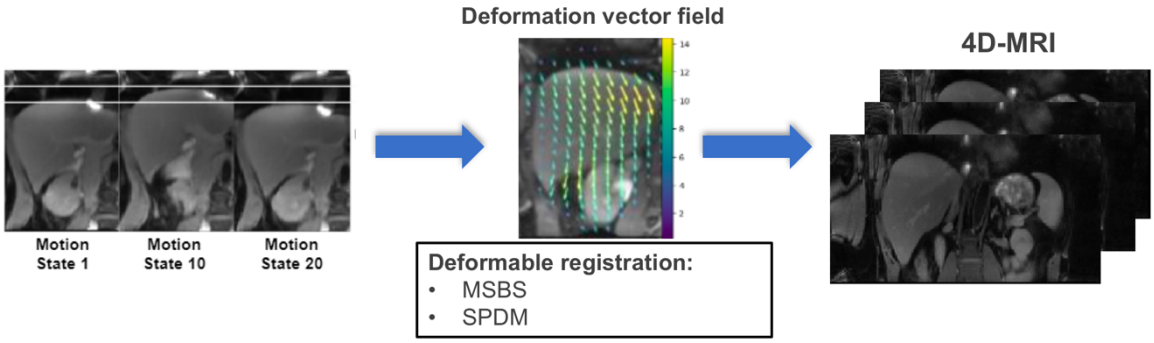

Figure 2. The process of improving image quality through deformable image registration. Using a reference volume, the deformation vector field (DVF) of sequential motion states are extracted, followed by deformable registrations. Two different deformable registration approaches are used here: (1) Multi-scale B-splines (MSBS) and (2) and subpixel deformation maps (SPDM).

(a)

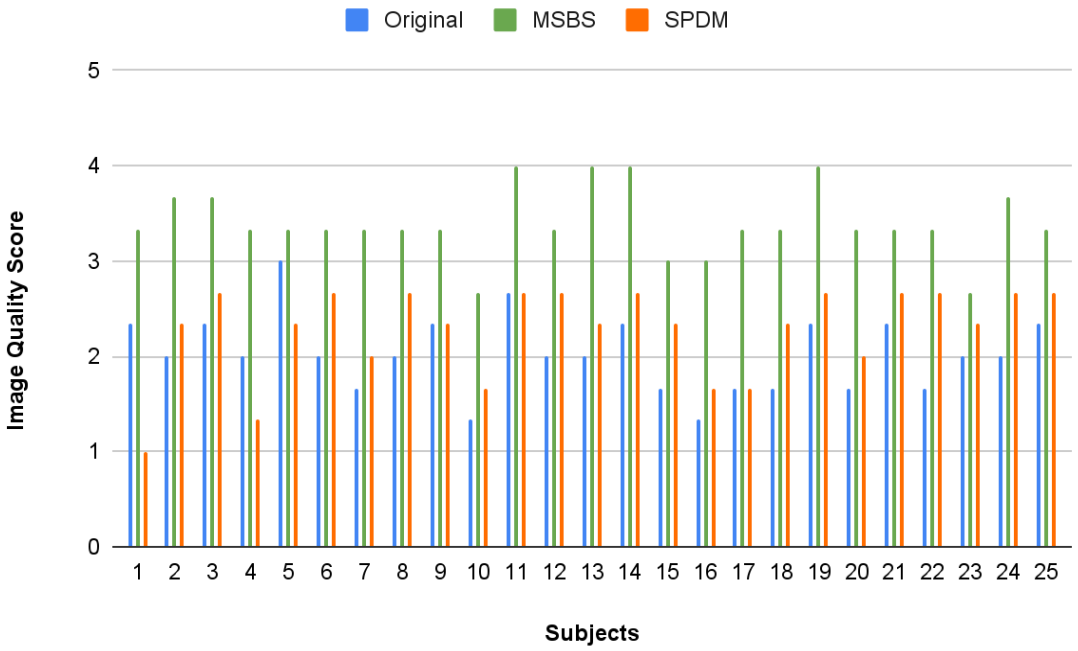

(b)

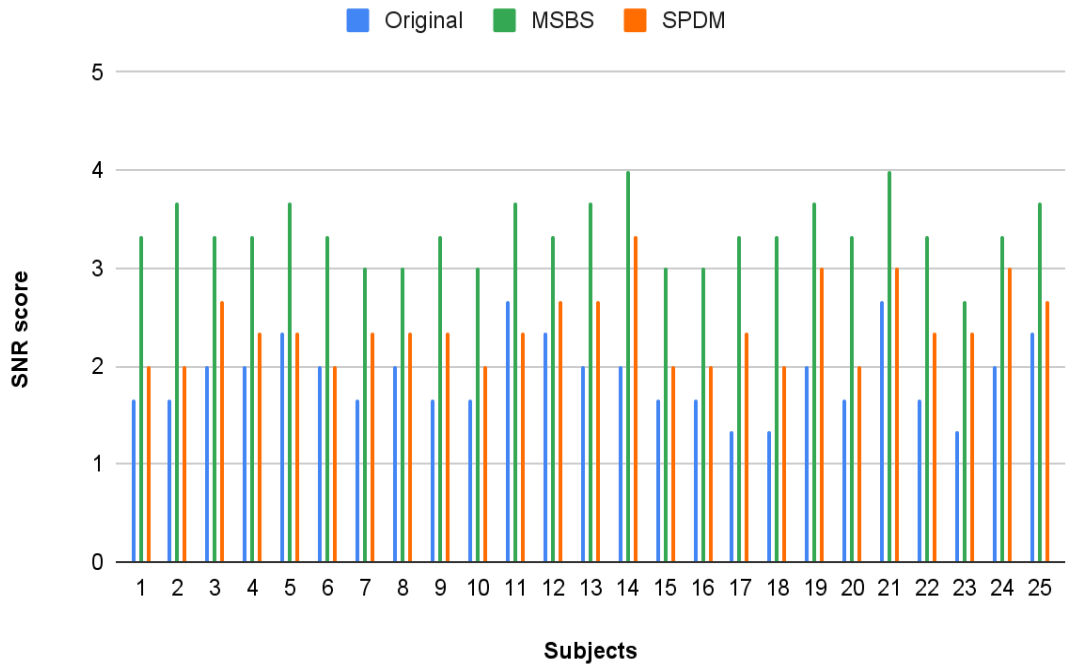

Figure 3. Comparison between original XD-GRASP, with the proposed manifold-regularized radial acquisition method using multi-scale B-splines approach (MSBS) and subpixel deformation maps (SPDM). **(a)** Average image quality score and **(b)** visual signal-to-noise ratio score of the 3 readers for 25 healthy subjects.

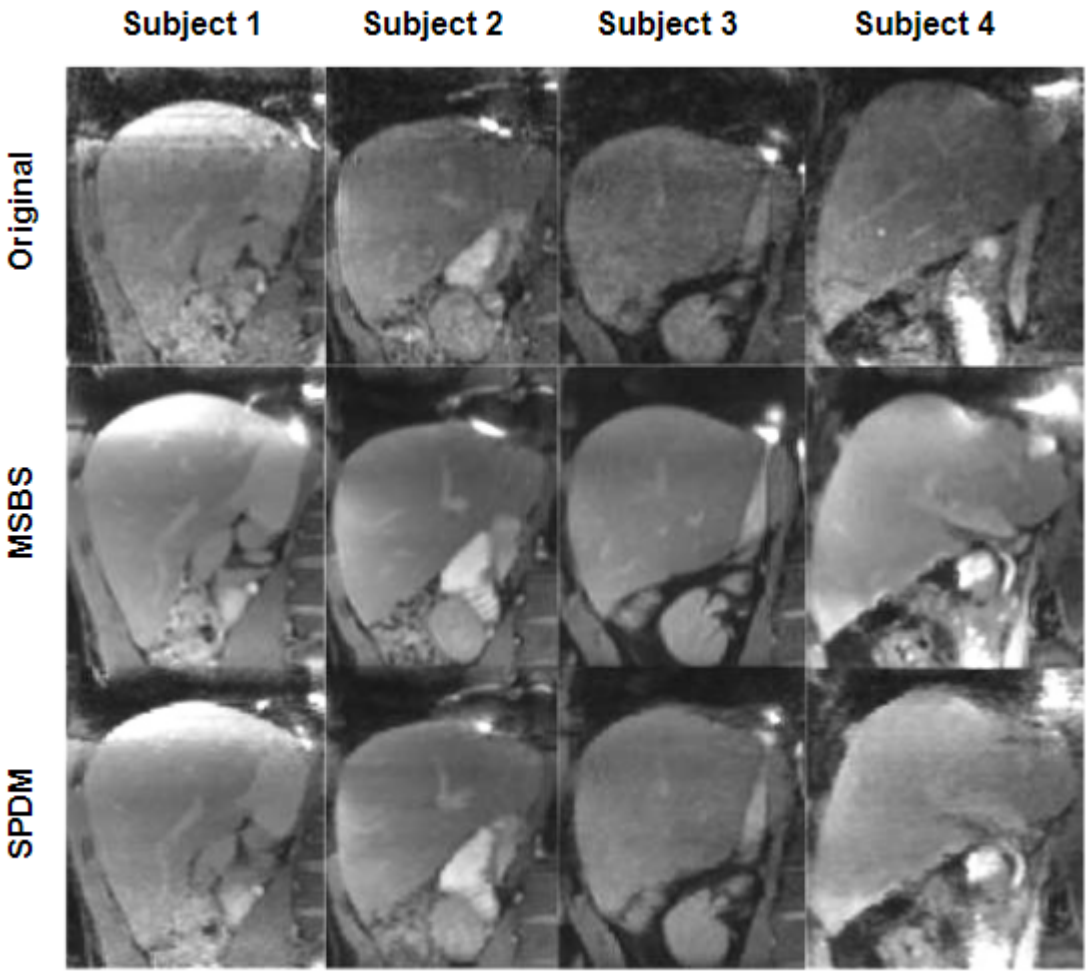

Figure 4. Example of reconstructed images for 4 different subjects with the proposed radial-based acquisition method, with and without registration.

805

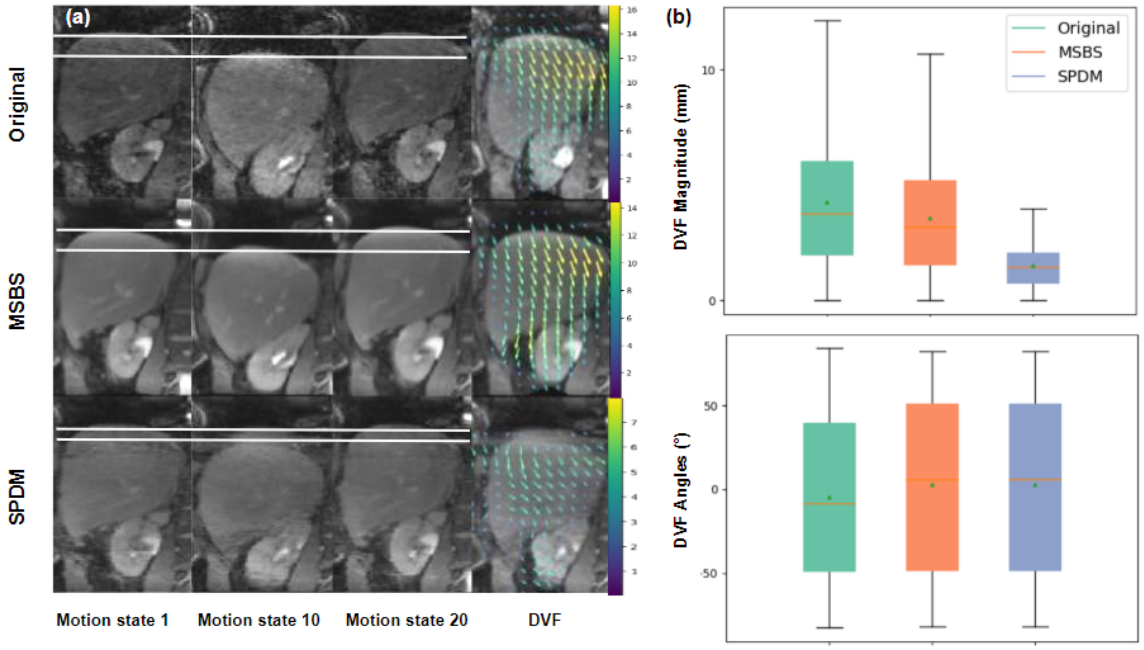

Figure 5. **(a)** Example of reconstructed images without registration, with a Multi scale B-splines approach and with a subpixel deformation maps approach at different liver positions from a 27-year-old healthy woman. Its representative deformation field vector (DVF) between inhale and exhale and **(b)** the corresponding DVF magnitude and angles distribution for all slices.

(a)

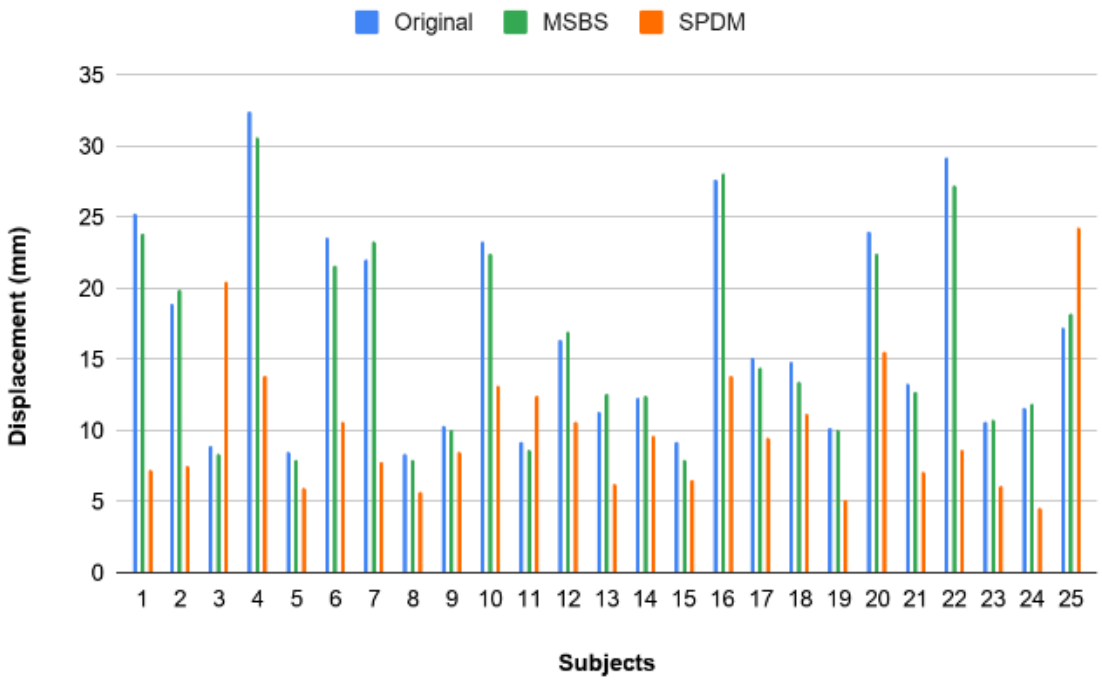

(b)

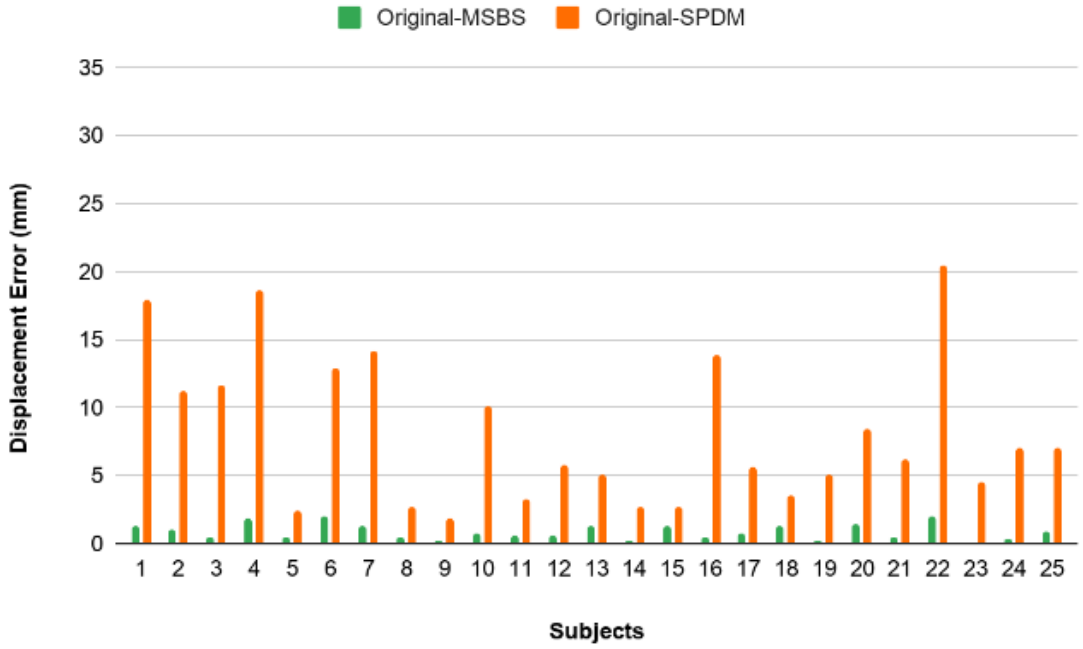

820

Figure 6. **(a)** Mean liver displacement between inhale and exhale for images without registration (Original), with MSBS approach and with SPDM approach measured from all healthy volunteers. **(b)** Error displacement between each method and the data without registration.

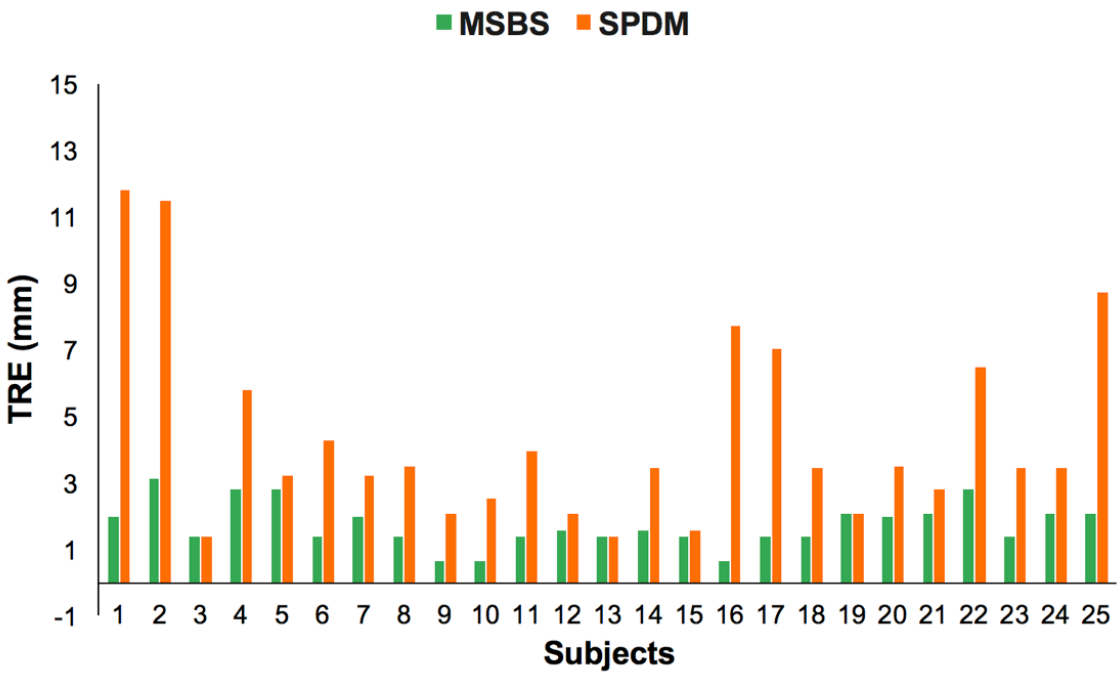

825

Figure 7. Target registration errors (TRE) for each subject, comparing the MSBS registration approach to the SPDM, which were integrated in the proposed radial free-breathing acquisition method.

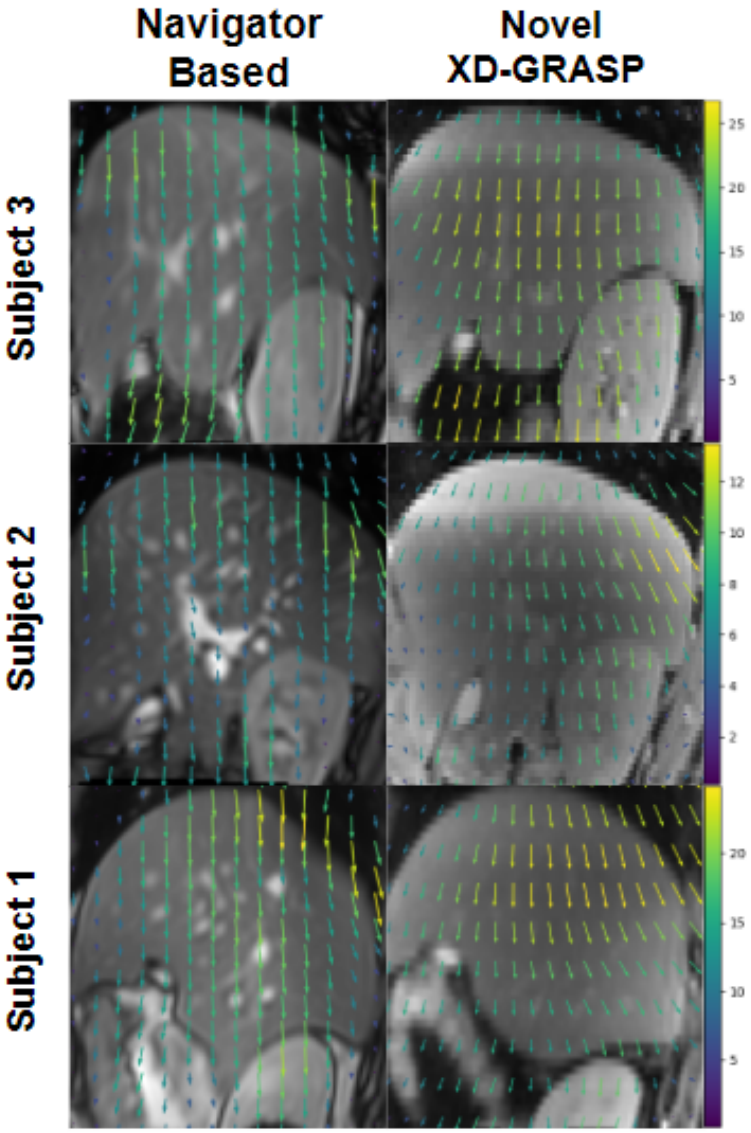

Figure 8. Sample deformation vector fields (DVF) for images reconstructed from 3 different healthy volunteers with the proposed radial acquisition method with manifold regularization, in comparison to a navigator based method.

(a)

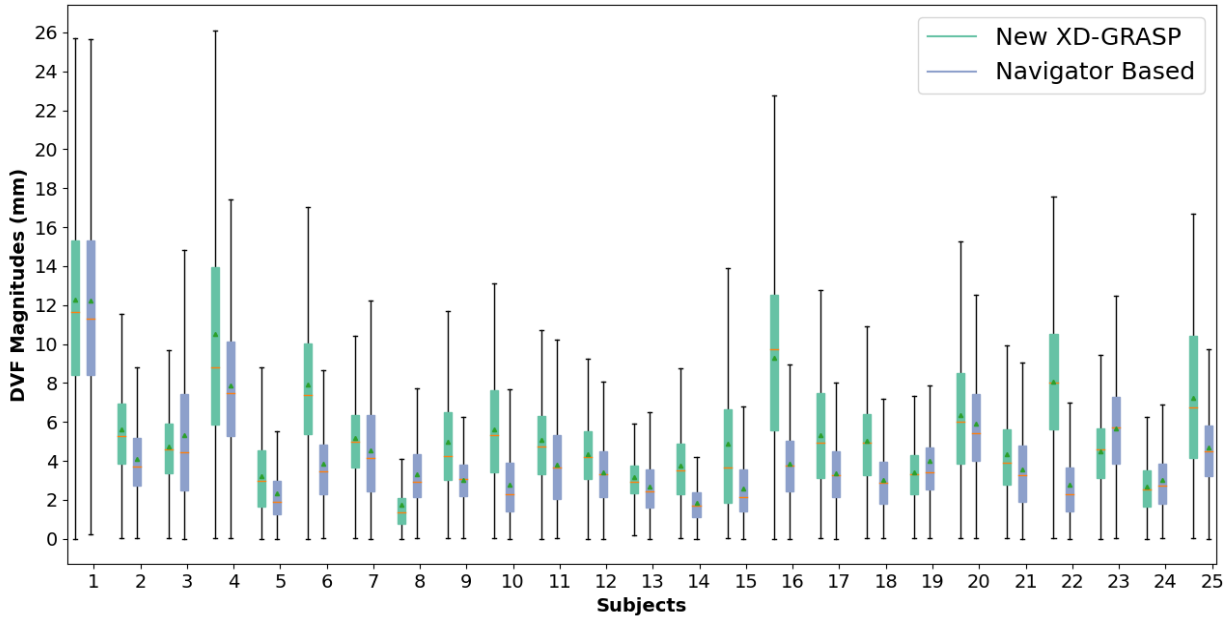

(b)

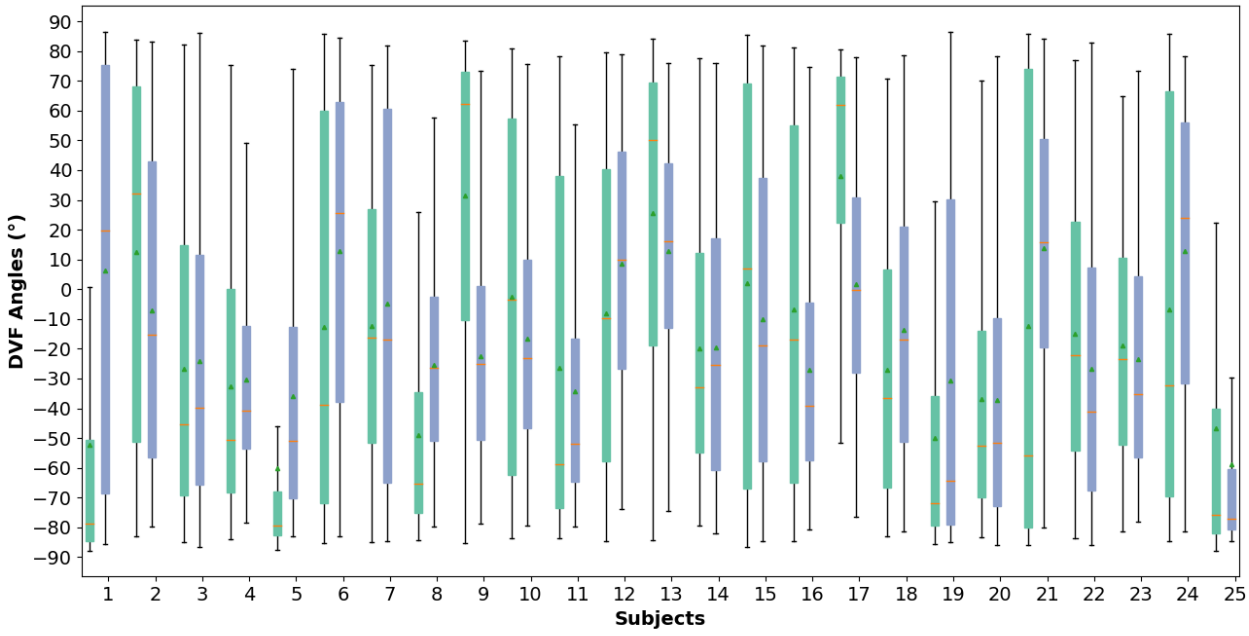

Figure 9. (a) Deformation vector fields (DVF) magnitudes and **(b)** angles distribution for images reconstructed with the proposed radial acquisition method for 25 healthy volunteers, in comparison to a navigator based method.

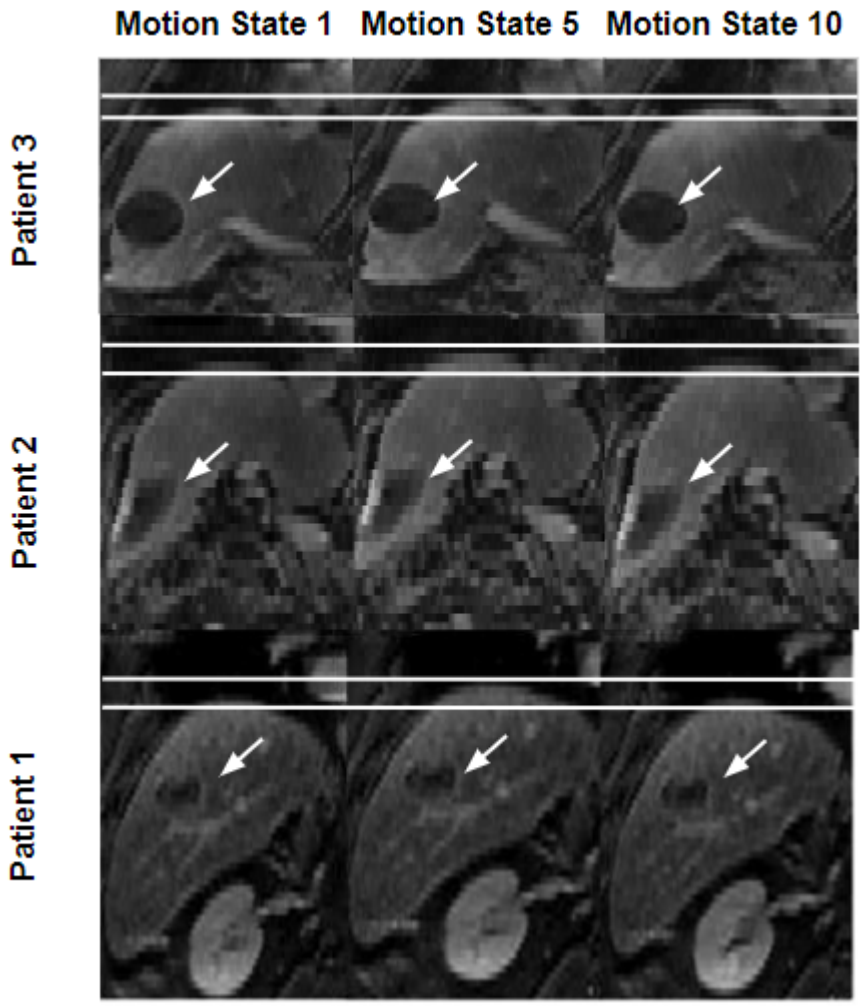

845 **Figure 10.** Examples of reconstructed images for 3 liver cancer patients with the proposed radial acquisition method using manifold regularization, combined with a multi-scale B-spline registration approach for different motion states (tumors identified by white arrow).